

8-2018

Deep-coverage whole genome sequences and blood lipids among 16,324 individuals

Pradeep Natarajan

Gina M. Peloso

Seyedeh M. Zekavat

May Montasser

Andrea Ganna

See next page for additional authors

Follow this and additional works at: https://scholarworks.utrgv.edu/som_pub



Part of the [Medicine and Health Sciences Commons](#)

Recommended Citation

Natarajan, P., Peloso, G.M., Zekavat, S.M. et al. Deep-coverage whole genome sequences and blood lipids among 16,324 individuals. *Nat Commun* 9, 3391 (2018). <https://doi.org/10.1038/s41467-018-05747-8>

This Article is brought to you for free and open access by the School of Medicine at ScholarWorks @ UTRGV. It has been accepted for inclusion in School of Medicine Publications and Presentations by an authorized administrator of ScholarWorks @ UTRGV. For more information, please contact justin.white@utrgv.edu, william.flores01@utrgv.edu.

Authors

Pradeep Natarajan, Gina M. Peloso, Seyedeh M. Zekavat, May Montasser, Andrea Ganna, Mark Chaffin, Amit V. Khera, John Blangero, Joanne E. Curran, and Michael C. Mahaney

ARTICLE

DOI: 10.1038/s41467-018-05747-8

OPEN

Deep-coverage whole genome sequences and blood lipids among 16,324 individuals

Pradeep Natarajan^{1,2,3}, Gina M. Peloso⁴, Seyedeh Maryam Zekavat^{5,6}, May Montasser⁷, Andrea Ganna^{3,8}, Mark Chaffin³, Amit V. Khera^{1,2,3}, Wei Zhou⁹, Jonathan M. Bloom^{3,8}, Jesse M. Engreitz^{3,10}, Jason Ernst¹¹, Jeffrey R. O'Connell⁷, Sanni E. Ruotsalainen¹², Maris Alver¹³, Ani Manichaikul¹⁴, W. Craig Johnson¹⁵, James A. Perry⁷, Timothy Poterba^{3,8}, Cotton Seed^{3,8}, Ida L. Surakka¹², Tonu Esko¹³, Samuli Ripatti¹², Veikko Salomaa¹², Adolfo Correa¹⁶, Ramachandran S. Vasan^{17,18,19}, Manolis Kellis^{3,20}, Benjamin M. Neale^{1,2,3,8}, Eric S. Lander³, Goncalo Abecasis²¹, Braxton Mitchell⁷, Stephen S. Rich¹⁴, James G. Wilson^{16,22}, L. Adrienne Cupples^{4,19}, Jerome I. Rotter²³
NHLBI TOPMed Lipids Working Group, Cristen J. Willer²⁴ & Sekar Kathiresan^{1,2,3}

Large-scale deep-coverage whole-genome sequencing (WGS) is now feasible and offers potential advantages for locus discovery. We perform WGS in 16,324 participants from four ancestries at mean depth >29X and analyze genotypes with four quantitative traits—plasma total cholesterol, low-density lipoprotein cholesterol (LDL-C), high-density lipoprotein cholesterol, and triglycerides. Common variant association yields known loci except for few variants previously poorly imputed. Rare coding variant association yields known Mendelian dyslipidemia genes but rare non-coding variant association detects no signals. A high 2M-SNP LDL-C polygenic score (top 5th percentile) confers similar effect size to a monogenic mutation (~30 mg/dl higher for each); however, among those with severe hypercholesterolemia, 23% have a high polygenic score and only 2% carry a monogenic mutation. At these sample sizes and for these phenotypes, the incremental value of WGS for discovery is limited but WGS permits simultaneous assessment of monogenic and polygenic models to severe hypercholesterolemia.

¹ Center for Genomic Medicine and Cardiovascular Research Center, Massachusetts General Hospital, Boston, MA 02114, USA. ² Department of Medicine, Harvard Medical School, Boston, MA 02115, USA. ³ Broad Institute of Harvard & MIT, Cambridge, MA 02142, USA. ⁴ Department of Biostatistics, Boston University School of Public Health, Boston, MA 02118, USA. ⁵ Yale School of Medicine, New Haven, CT 06510, USA. ⁶ Department of Computational Biology & Bioinformatics, Yale University, New Haven, CT 06520, USA. ⁷ School of Medicine, University of Maryland, Baltimore, MD 21201, USA. ⁸ Analytic and Translational Genetics Unit, Massachusetts General Hospital, Boston, MA 02114, USA. ⁹ Department of Computational Medicine and Bioinformatics, School of Public Health, University of Michigan, Ann Arbor, MI 48109, USA. ¹⁰ Society of Fellows, Harvard University, Cambridge, MA 02138, USA. ¹¹ Department of Biological Chemistry, University of California, Los Angeles, Los Angeles, CA 90095, USA. ¹² Institute for Molecular Medicine Finland, Helsinki 00290, Finland. ¹³ Estonian Genome Center, University of Tartu, Tartu 51010, Estonia. ¹⁴ Center for Public Health Genomics, University of Virginia, Charlottesville, VA 22908, USA. ¹⁵ Department of Biostatistics, University of Washington, Seattle, WA 98195, USA. ¹⁶ Department of Medicine, University of Mississippi Medical Center, Jackson, MS 39216, USA. ¹⁷ Sections of Preventive Medicine and Epidemiology and Cardiology, Department of Medicine, Boston University School of Medicine, Boston, MA 02118, USA. ¹⁸ Department of Epidemiology, Boston University School of Public Health, Boston, MA 02118, USA. ¹⁹ Framingham Heart Study, Framingham, MA 01702, USA. ²⁰ Computer Science and Artificial Intelligence Lab (CSAIL), Massachusetts Institute of Technology, Cambridge, MA 02139, USA. ²¹ Department of Biostatistics, School of Public Health, University of Michigan, Ann Arbor, MI 48109, USA. ²² Department of Physiology and Biophysics, University of Mississippi Medical Center, Jackson, MS 39216, USA. ²³ Institute for Translational Genomics and Population Sciences, LABioMed and Departments of Pediatrics and Medicine, Harbor-UCLA Medical Center, Torrance, CA 90502, USA. ²⁴ Departments of Human Genetics, Internal Medicine, and Computational Medicine and Bioinformatics, University of Michigan, Ann Arbor, MI 48109, USA. These authors contributed equally: Pradeep Natarajan, Gina M. Peloso, Seyedeh Maryam Zekavat. These authors jointly supervised this work: Cristen J. Willer, Sekar Kathiresan. Correspondence and requests for materials should be addressed to S.K. (email: skathiresan1@mgh.harvard.edu). A full list of consortium members appears at the end of the paper.

Plasma lipids, including total cholesterol, low-density lipoprotein cholesterol (LDL-C), high-density lipoprotein cholesterol (HDL-C), and triglycerides, are heritable risk factors for atherosclerotic cardiovascular disease^{1,2}. Understanding the inherited basis for plasma lipid levels has led to new treatments and to tests to identify individuals at risk for disease. Advances in technologies to characterize DNA sequence variants (i.e., Sanger sequencing, genotyping arrays, exome sequencing) have progressively allowed us to solve monogenic forms of dyslipidemia and to uncover common DNA sequence variants as well as rare mutations that contribute to plasma lipid levels in the population. However, due to the inherent limitations of genotyping arrays and exome sequencing, the non-coding regions of the genome remains incompletely characterized, particularly for rare mutations. In addition, the relative contribution of common DNA sequence variants and rare coding mutations to extreme lipid values in the population has not been delineated.

It is now possible to directly enumerate the whole-genome sequences of a large number of individuals. When performed at sufficient depth of coverage (>20-fold coverage per base), whole-genome sequencing (WGS) can detect single nucleotide polymorphisms (SNPs), insertions, and deletions across the allele frequency spectrum in both non-coding and coding regions. These advances allow us to test the incremental value of WGS as a tool for locus discovery and also develop a framework to understand why a specific individual might have an extreme lipid value. Toward these two goals, we studied the whole-genome sequences in 16,324 participants of European, African, East Asian, and Hispanic ancestries with available plasma lipid phenotypes.

In common variant association analyses, we replicate prior loci but detect newly associated variants not previously detected by prior genome-wide genotyping arrays or imputation. Analyses of rare coding variants yield known Mendelian dyslipidemia genes. Four approaches for analyzing rare non-coding variant associations do not detect any signals. WGS analysis of severe hypercholesterolemia shows a ten-fold enrichment of a high polygenic LDL-C score versus monogenic mutation for severe hypercholesterolemia. While the incremental value for WGS for locus discovery currently is limited largely due to relatively smaller sample sizes, WGS markedly improves the diagnostic yield of severe hypercholesterolemia through simultaneous assessment of monogenic and polygenic models.

Results

Deep-coverage WGS of 16,324 participants. Participants of the Framingham Heart Study (FHS), Old Order Amish (OOA), Jackson Heart Study (JHS), Multi-Ethnic Study of Atherosclerosis (MESA), FINRISK Study (FIN), and Estonian Biobank (EST) underwent WGS (Fig. 1). Following quality control (Supplementary Table 1), 16,324 participants with plasma lipids available were included in the analysis (Supplementary Table 2). The mean (standard deviation (SD)) age was 51 (15) years and 8669 (53%) were women. About 5911 (36%) of the participants were of non-European ancestry (Supplementary Table 2, Supplementary Fig. 1a-c). The proportion of individuals on lipid-lowering medications was low (9%).

WGS target coverage was >30X for FHS, OOA, JHS, and MESA (as a part of the NIH/NHLBI Trans-Omics for Precision

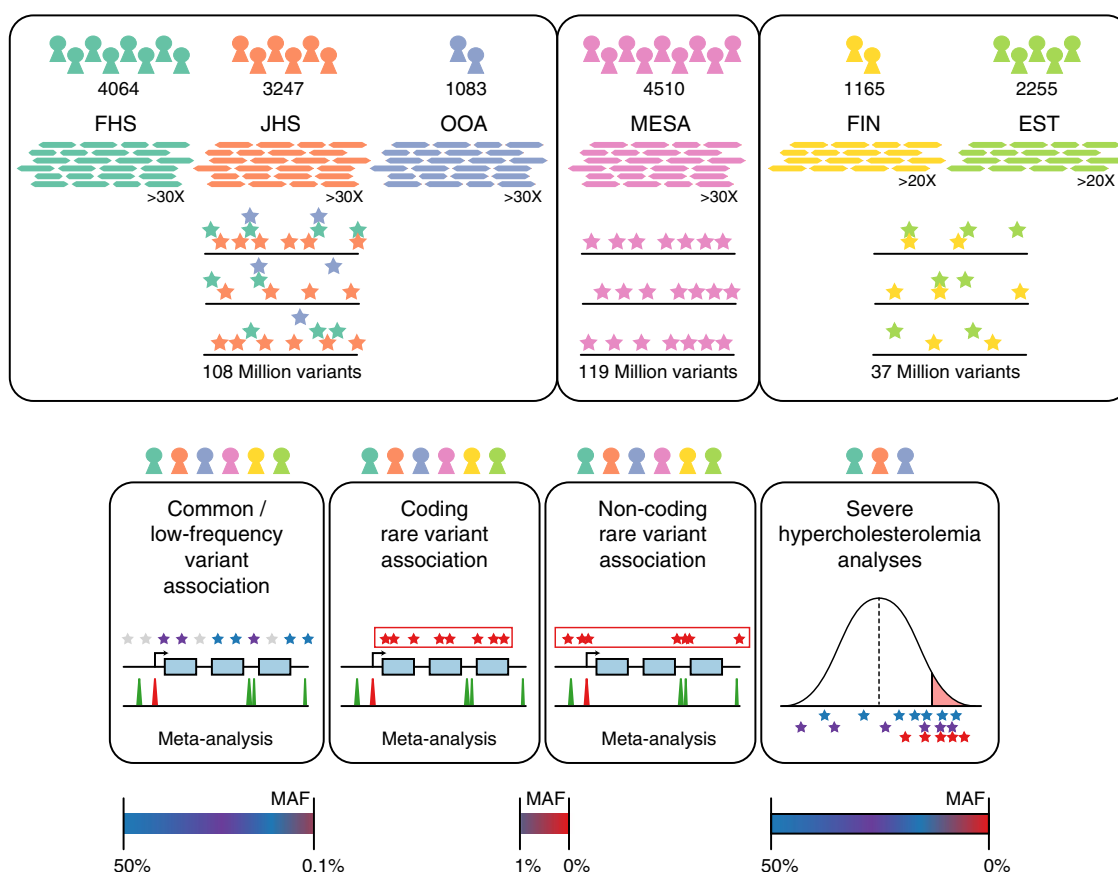


Fig. 1 Schematic of genomic variant discovery and analyses. Variants were jointly discovered in three distinct sets: (1) FHS, JHS, and OOA; (2) MESA; and (3) EST and FIN. Cohorts included in analyses are denoted by color-coded icons. Allele frequency spaces assessed are indicated for analyses. EST Estonia, FHS Framingham Heart Study, FIN Finland, JHS Jackson Heart Study, MESA Multi-Ethnic Study of Atherosclerosis, OOA Old Order Amish

Medicine (TOPMed) research program) and was $>20X$ for EST and FIN (Supplementary Fig. 2). The mean (SD) attained coverage for $>30X$ target samples was 37.1(5.4) X and for $>20X$ target was 29.8(5.4) X .

After performing quality control, a total of 189 million unique variants were discovered across all datasets. Total variant count characteristics varied by cohort due to sample sizes, relatedness, ethnicity, and population history (Fig. 2). As expected, the MESA cohort, of largely unrelated individuals of four diverse ethnicities, had the most variants per individual while the OOA cohort, a founder population of European ancestry, had the fewest variants per individual (Supplementary Table 3). The median number of variants, or sites with alleles differing from the hg19 reference genome, per individual was 3,391,000, of which on average 4878 were observed in only a single individual.

Common plus low-frequency variant association study. We first analyzed common and low-frequency variants, i.e., those that occur with enough minor alleles to provide robust individual association test statistics. We considered variants that had a minor allele frequency (MAF) $>0.1\%$ within at least one of the three WGS variant callsets (minor allele count >16 for the FHS/OOA/JHS callset, >9 for MESA, or >6 for FIN and EST) (Fig. 1). Association for these variants was estimated within each callset with each of the four plasma lipids levels, and then meta-analyzed using the inverse-variance method. Overall, 32,086,348 variants were included in this analysis. The test statistics were well controlled (Supplementary Table 4 and Supplementary Fig. 3a-d). We used a conventional statistical threshold for genome-wide significance ($\alpha = 5 \times 10^{-8}$)³ (Supplementary Fig. 3e-h). Using this cutoff, 592, 697, 447, and 522 variants were associated with total cholesterol, LDL-C, HDL-C, and triglycerides, respectively (Supplementary Table 5). These variants were distributed at 10, 7, 13, and 9 loci previously associated with total cholesterol, LDL-C, HDL-C, and triglycerides, respectively, and five at putative novel lipid loci (Supplementary Table 6)⁴⁻⁷. Of the variants at known loci, 12 (38.7%) were lead variants in prior associations, eight (25.8%) new lead variants were in high linkage disequilibrium (LD) ($r^2 > 0.8$) with prior lead variants, and the remaining 11 (35.5%) new lead variants were in low LD ($r^2 < 0.2$) with prior lead variants.

At a conventional α threshold of 5×10^{-8} , we discovered five associations at putative novel lipid loci (Supplementary Table 6).

For example, rs3215707 (MAF 2.0%), a 1-bp deletion at 9p24.1, was associated with HDL-C ($+3.3$ mg/dl, $P = 1.3 \times 10^{-8}$). rs3215707 occurs within an intron of *PLGRKT* and overlies active promoter and strong enhancer histone modification signals for HepG2 cells (Supplementary Fig. 4). The deletion is not in LD with any known SNPs and thus the association was not detectable by prior genome-wide association analyses. Within each callset, estimated effects were consistent (heterogeneity $P = 0.53$) and all demonstrated at least nominal association ($P < 0.05$) (Supplementary Table 7). We sought further replication for rs3215707 from additional independent samples. We interrogated 233 individuals from families with dyslipidemia and enriched for premature coronary heart disease who were whole-genome sequenced within the EUFAM study⁸. Using a mixed model, carriers (MAF 5.1%) were associated with a 5.6 mg/dl greater HDL cholesterol ($P = 0.03$).

We performed iterative conditional analyses to identify distinct independent associations among 16 loci reaching $P < 5 \times 10^{-8}$ for LDL-C, HDL-C, and triglycerides in the FHS/OOA/JHS (TOPMed Phase I) variant call file (VCF). While only four (25%) loci displayed evidence of allelic heterogeneity at $P < 5 \times 10^{-8}$, 13 (81.3%) had at least moderate evidence ($P < 1 \times 10^{-4}$) of allelic heterogeneity across the different ethnic groups available (Supplementary Table 8). Through conditional analyses for LDL-C, we identified a low-frequency haplotype specific to African Americans (MAF 0.1% FHS, 0% OOA, 1.0% JHS), including variants in LD ($r^2 > 0.8$) at a transcriptional transition region within the first intron of *LDLR* (rs17242843), *LDLR* promoter (rs17249141), and enhancer 4 kb upstream from the *LDLR* transcription start site (TSS) (rs114197570) (Supplementary Fig. 5, Supplementary Fig. 6). Presence of these variants resulted in a 28 mg/dl lowering of LDL-C ($P = 2 \times 10^{-11}$), suggesting increased expression of *LDLR* for carriers of the minor allele (Supplementary Fig. 7).

Rare variant association study of coding variants. To improve the power of detecting rare variant associations, we aggregated putative disruptive rare variants in coding sequences of each gene and tested the quantitative trait distribution among carriers of a set versus non-carriers⁹. We aggregated coding sequence variants within each gene that were predicted to lead to loss of function (e.g., nonsense, canonical splice-site, or frameshift) or annotated as “disruptive” by the ensemble MetaSVM¹⁰ in silico

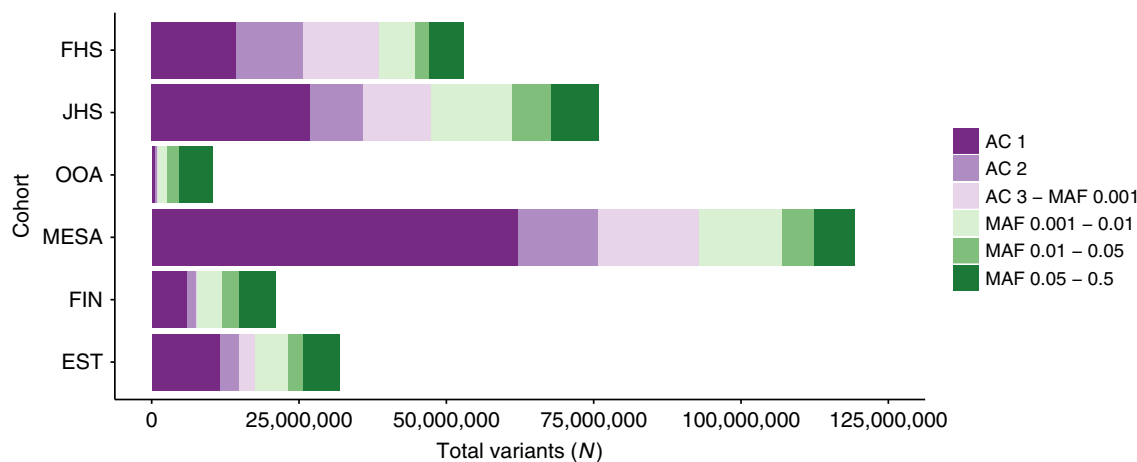


Fig. 2 Deep-coverage WGS identifies genomic variation across the allelic spectrum. Variant counts by allele count/frequency bin within each of the cohorts. Singletons (“AC 1”) and doubletons (“AC 2”) are separately distinguished from allele frequency bins within each cohort. Variants were jointly discovered in three distinct sets: (1) FHS, JHS, and OOA; (2) MESA; and (3) EST and FIN. AC allele count, EST Estonia, FHS Framingham Heart Study, FIN Finland, JHS Jackson Heart Study, MAF minor allele frequency, MESA Multi-Ethnic Study of Atherosclerosis, OOA Old Order Amish

approach. The median combined MAF per gene was 0.25% [interquartile range 0.090–0.69%] (Supplementary Fig. 8). To account for known bidirectional effects of disruptive mutations in some Mendelian dyslipidemia genes, we accordingly used a mixed model Sequence Kernel Association Test (SKAT)^{11,12}. Six genes associated with lipids at an exome-wide level ($\alpha = 0.05/ \sim 20,000$ protein-coding genes = 2.5×10^{-6}) (*LDLR*, *APOB*, *PCSK9*, and *APOE* for LDL-C, *LCAT* for HDL-C, and *APOC3* for triglycerides). Each has been previously established as a cause of Mendelian forms of dyslipidemia (Supplementary Table 9).

Rare variant association study of non-coding variants. Next, we sought to determine whether rare variants in non-coding regions associate with plasma lipids. We used four approaches to aggregate rare, non-coding variants. (Fig. 3). First, we aggregated variants within “sliding windows” of 3 kb in length^{13,14}. Second, we connected a non-coding variant to a gene if it resided in a segment annotated as an enhancer (and within 20 kb of a gene) or a region annotated as a promoter (and within 5 kb of the TSS of a gene). Third, using gene expression information, we connected a non-coding variant to a gene if it resided in a region annotated as an enhancer. Finally, we connected a non-coding variant to a gene based on a model which predicted gene-enhancer pairs using a chromatin-state model, including both HK27ac and Hi-C contact data, that we previously described¹⁵. Regulatory annotations were derived from the ENCODE and NIH Roadmap projects for two cell types—HepG2 and adipose nuclei—relevant to lipoprotein metabolism. For these analyses, we considered a $P < 0.05/254,032$ groups = 2.0×10^{-7} as significant (Supplementary Table 10, Supplementary Table 11).

Using the sliding window approach to non-coding burden tests, we observed suggestive associations for 3 kb windows at the *CETP* (start chr16:56667000) locus (minimum $P = 4 \times 10^{-6}$) and at the *APOA1-C3-A4-A5* (start chr11:117094500) locus (minimum $P = 8 \times 10^{-6}$) with HDL-C. A total of 17.6% of non-coding sliding windows occurring within 1 Mb of known lead lipid variants were at least nominally ($P < 0.05$) associated with lipids versus 4.4% in other regions of the genome across all traits (P difference = 8×10^{-272}).

An aggregation of rare non-coding variants at only two genes—*LDLR* and *APOE*—were associated with LDL-C and total cholesterol ($P < 2 \times 10^{-7}$) (Supplementary Fig. 9) (Supplementary Table 12). The strongest *LDLR* signal ($P = 9.7 \times 10^{-11}$) was seen for an analysis that connected enhancers and promoters to a gene based on physical proximity (approach #2 above). Closer inspection of the specific variants shows that this signal is driven by the low-frequency haplotype specific to African Americans also detected with single variant association (Supplementary Fig. 10) (Supplementary Table 12). The strongest *APOE* signal ($P = 8.1 \times 10^{-26}$) was observed in the model connecting enhancers to a gene by eQTLs for gene expression (approach #3 above). However, accounting for the strongest common variant association at the locus (rs7412, the *APOE* $\epsilon 2$ isoform allele), this signal attenuates to non-significance ($P = 1.8 \times 10^{-2}$), suggesting that the non-coding variants are driven by LD of the *APOE* $\epsilon 2$ isoform. Beyond these two results, we found no additional signals for a burden of non-coding variants.

Contribution of mono- and polygenic models to extreme LDL-C. With the availability of sequence in both coding and non-coding regions in the same samples, we estimated the simultaneous contribution of monogenic and polygenic

determinants to extreme LDL-C in a population-based sample of European (EA) and African (AA) ancestry. We defined “extreme” as the top or bottom 5th ancestry-specific percentile of LDL-C. Analyses were conducted in FHS and MESA-EA subjects (extreme cutoff as LDL-C > 183 mg/dl or LDL-C < 72.9 mg/dl) and JHS and MESA-AA subjects (extreme cutoff as LDL-C > 198.6 mg/dl or LDL-C < 71 mg/dl), separately.

Among participants with extremely high LDL-C, we searched for mutations in any of six Mendelian genes previously implicated as causing elevated LDL-C (*LDLR*, *APOB*, *PCSK9*, *ABCG5*, *ABCG8*, and *LDLRAP1*) (Supplementary Table 13).

To determine polygenic contribution, we implemented a systematic approach to derive, test, and validate a new “genome-wide” polygenic score for LDL-C using mutually independent datasets. A polygenic score provides a quantitative assessment of the cumulative risk associated with multiple common risk alleles for each individual.

We derived polygenic scores by three approaches: (1) only inclusion of genome-wide significant variants ($P < 5 \times 10^{-8}$ in separate discovery)⁷, (2) r^2 and P value thresholds to restrict variants without rescaling weights, and (3) entire summary results of 2M variants (LDpred) with rescaled weights based on r^2 and P values¹⁶. We derived polygenic scores based on the association statistics of all available common (MAF ≥ 0.01) SNPs with LDL-C, as determined by our previously published genome-wide association study⁷.

As a baseline, we generated an additional polygenic score restricted to lead variants ($P < 5 \times 10^{-8}$) at distinct genomic loci, weighted by discovery estimated effects (“restricted score”). Second, we applied various r^2 and P value thresholds to the previously published results. Finally, we used the LDpred computational algorithm which constructs genome-wide polygenic scores across full summary statistics¹⁶. Prior simulations have suggested that approaches additionally including variants with sub-genome-wide significance may improve the predictive capability of polygenic risk scores¹⁷. To include such variants, LDpred re-weights corresponding per-variant weights from our prior genome-wide association study⁷ based on LD, discovery P values, and a range of estimated causal fraction (e.g., non-zero effect sizes) markers. The correlation between the variants was assessed using the European reference population from the 1000 Genomes study¹⁷. The best score was determined based on maximal model fit (R^2) from a linear regression models in a health-care biobank of 25,534 unrelated individuals (Nord-Trøndelag Health Study, HUNT)¹⁸ (Supplementary Table 14).

For LDL-C, a genome-wide polygenic score incorporating 2 million SNPs with LDpred provided the best model fit (Supplementary Table 15). Compared to a restricted score of 59 SNPs independently significant associated with LDL-C, a relative increase of 21.6% of LDL-C variance was explained by the expanded 2M-SNP score ($r^2_{\text{restricted}} = 0.245$ vs. $r^2_{\text{expanded}} = 0.298$). We applied this polygenic score separately within the WGS samples in FHS, JHS, and MESA. We labeled individuals as having a high polygenic score if they fell in the top 5th percentile of race-specific score distributions (Tables 1 and 2).

Among EA participants, a monogenic mutation was associated with an odds ratio of 10.92 (95% CI 3.71(32.14) for extremely high LDL-C, whereas a high polygenic score associated with an odds ratio of 7.65 (95% CI 5.56–10.52). In EA individuals, those who carried a monogenic mutation had 30 mg/dl higher LDL-C (when compared with non-carriers; $P = 2.1 \times 10^{-4}$) and those who had a high polygenic score had 33 mg/dl greater LDL-C (when compared with all others; $P = 1.7 \times 10^{-57}$). Of the 287 EA participants with extremely high LDL-C, 2% carried a monogenic mutation and 23% had a high polygenic score.

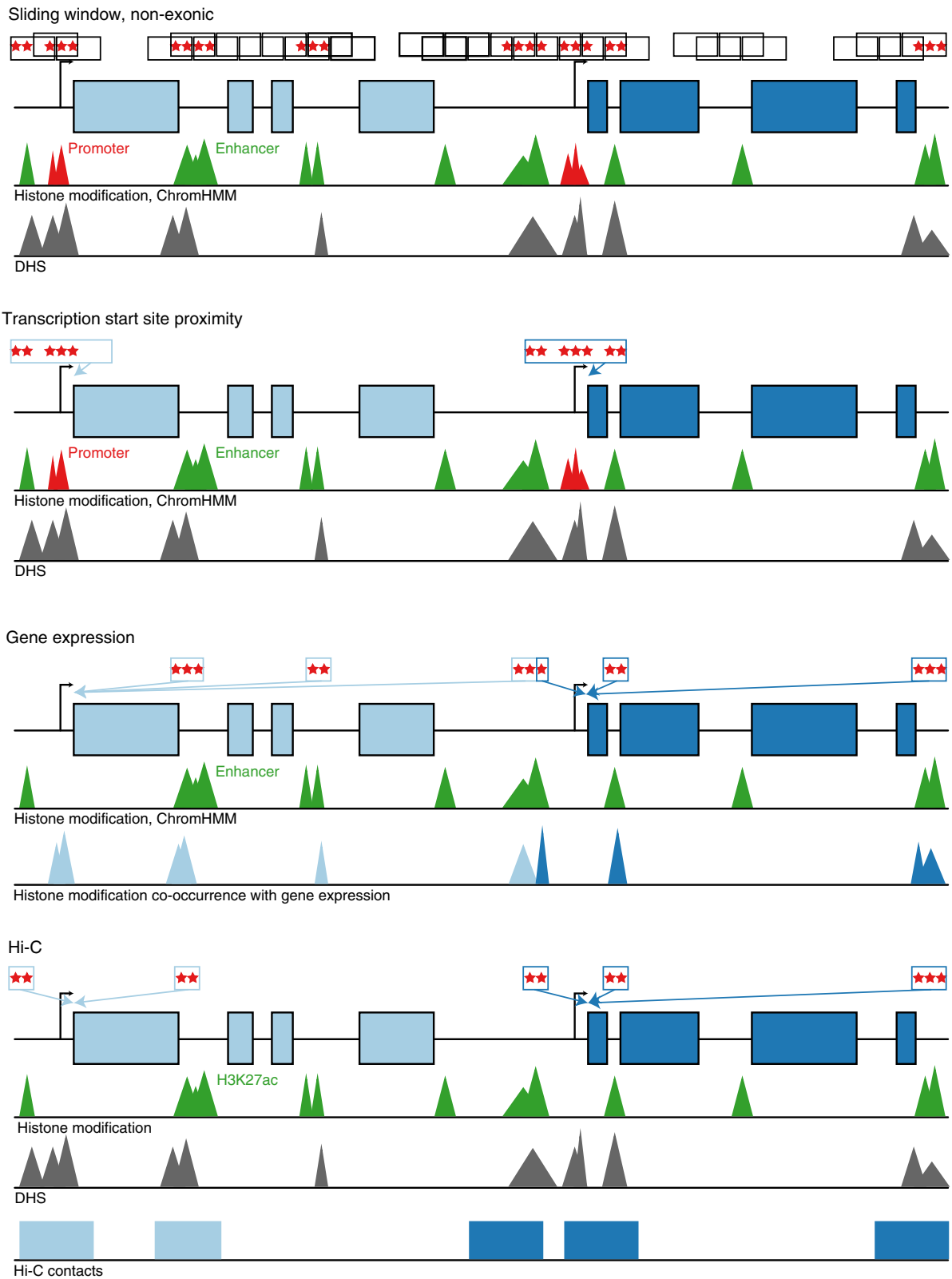


Fig. 3 Schematic of non-coding rare variant analyses. Four grouping schematics of rare non-coding variants (MAF <1%). (1) The sliding window approach tiles across the genome at fixed widths, only including variants overlying annotations consistent with enhancers, promoters, and DHS in non-exonic regions. All other approaches attempt to map non-coding putative functional genomic regions with discrete genes as the analytical unit. Overall, they are based on: (2) promoter, enhancer, and DHS annotations near a gene’s transcription start site, (3) co-occurrence of enhancer and DHS annotations with HepG2 gene expression, and (4) H3K27ac marks within Hi-C contact regions mapped to genes. DHS DNase hypersensitivity site, MAF minor allele frequency

Table 1 Effect of monogenic mutation or polygenic score on odds for extremely high or low LDL-C

Extremely high LDL-C											
Ancestry	N_{total}	$N_{extreme}$	Monogenic carrier ($N_{extreme}$)	High polygenic score ($N_{extreme}$)	Monogenic carrier OR (95% CI)	Monogenic carrier P-value	Monogenic carrier PAF	High polygenic score OR (95% CI)	High polygenic score P-value	Top 5th percentile of polygenic score PAF	
EA	5910	284	5	64	10.92 (3.71, 32.14)	1.4×10^{-5}	1.60	7.65 (5.56, 10.52)	5.7×10^{-36}	19.6	
AA	4380	217	7	29	7.43 (3.01, 18.35)	1.4×10^{-5}	2.79	3.2 (2.1, 4.89)	6.7×10^{-8}	9.2	
Extremely Low LDL-C											
Ancestry	N_{total}	$N_{extreme}$	Monogenic carrier ($N_{extreme}$)	Low polygenic score ($N_{extreme}$)	Monogenic carrier OR (95% CI)	Monogenic carrier P-value	Monogenic carrier PAF	Low polygenic score OR (95% CI)	Low polygenic score P-value	Bottom 5th percentile of polygenic score PAF	
EA	5910	286	6	82	21.73 (6.2, 76.15)	1.5×10^{-6}	2.00	10.38 (7.69, 14.02)	1.5×10^{-52}	25.9	
AA	4380	218	11	32	13.83 (6.25, 30.62)	9.4×10^{-11}	4.68	3.7 (2.46, 5.58)	3.9×10^{-10}	10.7	

Values are represented as OR [95% CI] for association with given trait. (b). Effect of monogenic mutation or polygenic score on LDL-C in mg/dl. Values are represented as beta [95% CI] in mg/dl for LDL-C. Multi-variable associations were performed with sex + age + age² (effects not listed) with monogenic carrier status + high polygenic score using logistic regression. Polygenic risk score was derived from 2 million variants using LDpred. High polygenic score was defined as membership in the top 5th percentile of the ancestry-specific score distribution. AA, African American; EA, European American; SE, standard error.

Table 2 Effect of monogenic mutation or polygenic score on LDL-C in mg/dl

Monogenic mutation or high polygenic score										
Ancestry	N_{total}	Monogenic carrier (N)	High polygenic score (N)	Monogenic carrier β (mg/dl)	Monogenic carrier SE	Monogenic carrier P-value	High polygenic score β (mg/dl)	High polygenic score SE	High polygenic score P-value	
EA	5910	18	297	29.98	8.07	2.1×10^{-4}	33.07	2.05	1.7×10^{-57}	
AA	4380	25	220	41.05	7.93	2.3×10^{-7}	16.96	2.74	6.4×10^{-10}	
Monogenic mutation or low polygenic score										
Ancestry	N_{total}	Monogenic carrier (N)	Low polygenic score (N)	Monogenic carrier β (mg/dl)	Monogenic carrier SE	Monogenic carrier P-value	Low polygenic score β (mg/dl)	Low polygenic score SE	Low polygenic score P-value	
EA	5910	12	297	-47.25	9.55	7.7×10^{-7}	-35.00	2.00	7.9×10^{-67}	
AA	4380	28	220	-41.41	7.47	3.1×10^{-8}	-20.41	2.74	1.1×10^{-13}	

Values are represented as beta [95% CI] in mg/dl for LDL-C. Multi-variable associations were performed with sex + age + age² (effects not listed) with monogenic carrier status + high polygenic score using linear regression. Polygenic risk score was derived from 2 million variants using LDpred. High polygenic score was defined as membership in the top 5th percentile of the ancestry-specific score distribution. AA, African American; EA, European American; SE, standard error.

Among AA participants, a monogenic mutation was associated with an odds ratio of 7.43 (95% CI 3.01–18.35) for extremely high LDL-C, whereas a high polygenic score associated with an odds ratio of 3.2 (95% CI 2.1–4.89). In AA individuals, those who carried a monogenic mutation had 41 mg/dl higher LDL-C (when compared with non-carriers; $P = 2.3 \times 10^{-7}$), greater than that observed among EA individuals, and those who had a high polygenic score had 17 mg/dl greater LDL-C (when compared with all others; $P = 6.4 \times 10^{-10}$), less than the effect observed among EA individuals. Of the 217 AA participants with extremely high LDL-C, 3% carried a monogenic mutation and 13% had a high polygenic score. Across the full spectrum of LDL-C polygenic score, every SD of the LDL-C polygenic score was associated with 15.5 mg/dl LDL-C among EA ($P = 4 \times 10^{-277}$) and 8.7 mg/dl LDL-C among AA ($P = 1 \times 10^{-47}$).

We replicated the association between a high polygenic score and extremely high LDL-C in an independent sample, the ARIC

cohort. Among ARIC-EA ($N = 7755$) individuals, a high polygenic score was associated with an odds ratio of 7.35 (95% CI 5.95–9.10; $P < 2 \times 10^{-16}$) for extremely high LDL-C and 42.8 mg/dl (95% CI 40.0–47.5; $P < 2 \times 10^{-16}$) higher LDL-C compared with individuals without a high polygenic score. Among ARIC-AA ($N = 1907$) participants, a high polygenic score was associated with an odds ratio of 2.7 (95% CI 1.77–4.09; $P < 3.3 \times 10^{-6}$) for extremely high LDL-C and a 23.2 mg/dl (95% CI 15.0–31.5; $P = 3.8 \times 10^{-8}$) higher LDL-C compared with individuals without a high polygenic score.

We analyzed the monogenic and polygenic contribution to extremely low LDL-C in EA and AA participants and found similar patterns where monogenic mutations as well as a polygenic score conferred similar effect sizes (Tables 1 and 2).

Discussion

We performed WGS in 16,342 ethnically diverse individuals and analyzed the incremental value of WGS for locus discovery

for blood lipid levels and for clinical interpretation. We replicated associations for 28 common variant loci previously associated with lipids in much larger genome-wide association analyses. We identified an association for a low frequency 1-bp deletion at 9p24.1 with HDL-C. We replicated burden associations of rare coding mutations at known Mendelian lipid genes. However, we did not detect any burden associations of rare non-coding mutations through four different approaches. Lastly, we developed a genome-wide polygenic score and showed that such a score confers an effect size on LDL-C similar to carrying a monogenic mutation and is present in ten-fold more individuals with severe hypercholesterolemia than monogenic mutations. At these sample sizes and for these phenotypes, the incremental value of WGS as a discovery tool was limited but WGS allowed us to simultaneously assess the contribution of monogenic and polygenic models to severe hypercholesterolemia.

These results permit several conclusions. Using WGS as a discovery tool, the incremental yield of new loci was modest. Current sample sizes for WGS are much smaller compared to genome-wide association and whole exome sequencing studies clearly limiting relative power for detecting associations for common/low-frequency non-coding variants and rare coding variants. Despite genome-wide interrogation of rare variant signals in non-coding space, we identified no burden-of-rare-variant signals using four different aggregation approaches and regulatory annotations from two relevant tissues.

Mutation target size and natural selection pressure are smaller in non-coding regions when compared with coding regions; based on these considerations, power calculations have suggested that sample sizes may need to be considerably larger to identify rare variant burden associations in non-coding regions compared to coding regions⁹. While sample size is an important determinant of power, prioritization of putative causal rare non-coding variants remains a major power limitation. Functional annotations from reference datasets largely prioritize functional sequence and MAF thresholds assist in prioritizing causal variants, but this likely retains a large fraction of benign variants. Genome-wide organism-level functional variant scores¹⁹ offer the promise of improved prioritization but did not improve associations at *LDLR* and *APOE*. Novel, genome-wide tissue-level functional scores may improve prioritization compared to organism-level scores^{20–22}. Assessments of consequence for rare coding mutations in experimental systems has improved associations of lipid-related genes beyond in silico tools^{23,24}. Similar systematic approaches for rare non-coding variants in relevant tissues may further improve power.

WGS in diverse populations permits discovery of novel associated variants. Most of the observed lead single variant associations at known loci were previously tagged by lead variants from genome-wide association analyses of largely European ancestry participants. Our trans-ethnic analyses yielded new lead variants at one-third of known lipid loci not previously tagged by prior lead loci. Additionally, variant classes not previously detected by array-genotyping and whole-exome sequencing are associated with lipids. We observed that a 1-bp deletion, not correlated with previously cataloged variants, was associated with HDL cholesterol. These observations indicate that new variants are detected not only by including diverse ethnicities, but also WGS can overcome many limitations of imputation for variant discovery, including application in non-Europeans, variable coverage in genome-wide genotype arrays, and detection of rarer variants.

Of great interest, we observed that the relative contribution of polygenic score to extremely high LDL-C is considerably greater than monogenic mutations. For example, in EA individuals, both high polygenic score and a monogenic mutation confer similar effects (~30 mg/dl higher LDL-C) but a high polygenic score is

present in 20% of participants with extremely high LDL-C whereas a monogenic mutation is present in only 2%. In most individuals who carry diagnosis of familial hypercholesterolemia, no monogenic mutation is identified with clinical exome sequencing^{25,26} for a large fraction of these “mutation-negative” familial hypercholesterolemia, high polygenic scores may be operative. WGS permits the application of simultaneous assessment of monogenic determinants as well as the most optimally performing polygenic score with relative ease.

Our observed monogenic carrier rates for severe hypercholesterolemia (2%) are consistent with observations in other population-based cohorts^{26,27} and health-care-associated biobanks²⁵ but lower than for patients with clinical criteria for familial hypercholesterolemia (up to 24%)²⁷, particularly those clinically referred for familial hypercholesterolemia genetic testing (up to 50%)^{28–31}. As anticipated, this subgroup is also likely to have a greater monogenic relative to polygenic contribution^{32,33}.

Important limitations should be considered. First, appropriate definitions of statistical significance for WGS association analyses have not been harmonized in the field. The convention of $\alpha = 5 \times 10^{-8}$ comes from the assumption of performing 1,000,000 independent tests. Based on our findings and simulations from others³, 10^{-9} may be more appropriate for analyses across diverse ethnicities to allele frequency 0.1%. Second, power is somewhat diminished with our rare variant meta-analysis approach to combine *P* values with Fisher’s method. Given known diverse coding mutations within Mendelian genes with bidirectional effects and the inability to assume unidirectional effects within the non-coding space, we employed a SKAT statistical framework. Prior approaches leveraging covariance matrices for SKAT meta-analysis were computationally inefficient for the dataset and multiple grouping strategies^{34,35}. Thus, our approach is conservative. Third, the polygenic scores described here were derived from genome-wide association studies performed largely in EA ancestry participants⁷. Because allele frequencies, LD patterns, and effect sizes of common polymorphisms vary by ancestry, the predictive capacity of polygenic score was attenuated in non-European ancestry individuals³⁶. Furthermore gene flow between ancestral groups and resultant admixture^{37,38} for an individual further hinders accuracy of polygenic risk scores derived from distinct populations for application at the individual level³⁹. This is an important limitation for the field that requires efforts to characterize common genomic variation influencing complex traits among non-Europeans and develop locus admixture-aware polygenic risk scoring.

In summary, we present a large-scale WGS analysis of plasma lipids in 16,324 ethnically diverse participants. Common, non-coding variants and rare, coding variants contribute to plasma lipid variation; however, association signals for rare, non-coding mutations were not detectable. Among participants with severe hypercholesterolemia, a high polygenic score was present in ten-fold more individuals than a monogenic mutation.

Methods

Study participants. Study participants were from the FHS (*N* = 4064), JHS (*N* = 3247), OOA (*N* = 1083), MESA (*N* = 4510), FIN (*N* = 1165), and the EST (*N* = 2255). Each study was previously approved by respective institutional review boards (IRBs), including for the generation of WGS data and association with phenotypes. All participants provided written consent. The analyses of WGS data with plasma lipids was approved by the Massachusetts General Hospital IRB (MGH IRB# 2016P001308). Please refer to Supplementary Note 1 for study participant details.

WGS, variant calling, and genotyping. Sequencing was performed at one of the four sequencing centers, with all members within a cohort sequenced at the same center. For the TOPMED phase 1 data, 4148 FHS individuals and 1095 OOA individuals were sequenced at the Broad Institute of Harvard and MIT (Cambridge,

MA), while 3266 JHS individuals were sequenced at University of Washington Northwest Genomics Center (Seattle, WA). About 4601 MESA individuals were additionally sequenced at the Broad Institute of Harvard and MIT as part of TOPMed Phase 2. About 1180 Finnish FINRISK individuals and 2281 Estonian Biobank participants were sequenced at the Broad Institute of Harvard and MIT (Cambridge, MA). Three separate callsets were utilized due to timeline of availability as well as data use restrictions.

TOPMed phase 1 BAM files provided by the sequencing centers were harmonized by the TOPMed Informatics Research Center (IRC) before joint variant discovery and genotype calling across studies. In brief, sequence data were received from each sequencing center in the form of bam files mapped to the 1000 Genomes hs37d5 build 37 decoy reference sequence. Processing was coordinated and managed by the “GotCloud” processing pipeline⁴⁰.

The two sequence quality criteria used in order to pass sequence data on for joint variant discovery and genotyping are: estimated DNA sample contamination below 3%, and fraction of the genome covered at least $10 \times 95\%$ or above. DNA sample contamination was estimated from the sequencing center read mapping using software `verifyBamId`⁴¹.

The genotype callsets used for analysis are from “freeze 3a” of the variant calling pipeline performed by the TOPMed IRC (Center for Statistical Genetics, University of Michigan, Hyun Min Kang, Tom Blackwell, and Goncalo Abecasis). The software tools used in this version of the pipeline are available in the following repository: https://github.com/statgen/topmed_freeze3_calling. Variant detection (SNPs and indels) from each sequenced (and aligned) genome is performed by `vt discover2` software tool⁴². The variant calling software tools are under active development; updated versions can be accessed at <http://github.com/atks/vt> or <http://github.com/hyunminkang/apigenome>.

WGS for MESA, FINRISK, and the Estonian Biobank was performed using the Illumina HiSeqX platform at the Broad Institute of Harvard and MIT (Cambridge, MA). DNA samples are informatically received into the Genomics Platform’s Laboratory Information Management System via a scan of the tube barcodes using a Biosero flatbed scanner. All samples are then weighed on a BioMicro Lab’s XL20 to determine the volume of DNA present in the sample tubes. Following this, the samples are quantified in a process that uses PICO-green fluorescent dye. Once volumes and concentrations are determined, the samples are then handed off to the Sample Retrieval and Storage Team for storage in a locked and monitored -20°C walk-in freezer.

Libraries were constructed and sequenced on the Illumina HiSeqX with the use of 151-bp paired-end reads for WGS and output was processed by Picard to generate aligned BAM files (to hg19)^{43,44}. Samples were tracked by automated LIMS messaging. Samples were fragmented with acoustic shearing and libraries were prepared with a KAPA Biosystems kit. Libraries were normalized to 1.7 nM. Cluster amplification was performed using Illumina cBot and flowcells were sequenced in HiSeq X. Variants (SNPs and indels) were discovered using the Genome Analysis Toolkit (GATK) v3 HaplotypeCaller according to Best Practices⁴⁵. Variants from MESA samples were generated in one callset. Finland and Estonia samples were jointly called in a separate callset.

Whole-genome sequence quality control. The following three approaches were used by the TOPMed Genetic Analysis Center to identify and resolve sample identity issues: (1) concordance between annotated sex and biological sex inferred from the WGS data, (2) concordance between prior SNP array genotypes and WGS-derived genotypes, and (3) comparisons of observed and expected relatedness from pedigrees.

The variant filtering in TOPMed Freeze 3 were performed by (1) first calculating Mendelian consistency scores using known familial relatedness and duplicates and (2) training SVM classifier between the known variant sites (positive labels) and the Mendelian inconsistent variants (negative labels). Two additional hard filters were applied: (1) Excess heterozygosity filter (EXHET), if the Hardy–Weinberg disequilibrium P -value was less than 1×10^{-6} in the direction of excess heterozygosity. An additional ~ 3900 variants were filtered out by this filter, and (2) Mendelian discordance filter (DISC), with 3 or more Mendelian inconsistencies or duplicate discordances observed from the samples. An additional $\sim 370,000$ variants were filtered out by this filter. Functional annotation for each variant was provided in the INFO field using `snPEff 4.1` with a GRCh37.75 database⁴⁶. Analysis used hard-call genotypes, without genotype likelihoods. Genotypes with a depth < 10 were excluded.

Additional measures for quality control of TOPMed Phase I Freeze 3 and quality control for MESA, Finland, and Estonia were performed using the Hail software package (<https://hail.is>)⁴⁷. Samples were filtered by contamination ($> 3.0\%$ for all, except $> 5.0\%$ for Finland and Estonia), chimeras $> 5\%$, GC dropout > 4 , raw coverage ($< 30X$ for all, except $< 19X$ for Finland and Estonia), indeterminate genotypic sex or genotypic/phenotypic sex mismatch.

Variants for MESA, Finland, and Estonia were initially filtered by GATK Variant Quality Score Recalibration. Additionally, genotypes with $GQ < 20$, $DP < 10$ or > 200 , and poor allele balance (homozygous with < 0.90 supportive reads or heterozygous with < 0.20 supportive reads) were removed. And variants within low complexity regions were removed across all samples⁴⁸. Variants with $> 5\%$ missing calls, quality by depth < 2 (SNPs) or < 3 (indels), `InbreedingCoeff` < -0.3 , and `pHWE` $< 1 \times 10^{-9}$ (within each cohort) were filtered out.

Annotation. Variants were annotated with Hail using annotations from Ensembl’s Variant Effect Predictor⁴⁹ for protein-coding annotations and Reg2Map HoneyBadger2-intersect for regulatory annotations at DNase I regions $-\log_{10}(P) \geq 10$ (https://personal.broadinstitute.org/meuleman/reg2map/HoneyBadger2-intersect_release/).

Traits. Conventionally measured plasma lipids, including total cholesterol, LDL-C, HDL-C, and triglycerides, were included for analysis. LDL-C was either calculated by the Friedewald equation when triglycerides were < 400 mg/dl or directly measured. Given the average effect of statins, when statins were present, total cholesterol was adjusted by dividing by 0.8 and LDL-C by dividing by 0.7, as previously done⁵⁰. Triglycerides were natural log transformed for analysis. Phenotypes were harmonized by each cohort and deposited into the dbGaP TOPMed Exchange Area.

Common plus low-frequency variant association analysis. Single variant analysis was performed in EPACTS (<https://genome.sph.umich.edu/wiki/EPACTS>) with Efficient Mixed-Model Association eXpedited (EMMAX) for associating each variant site with each lipid trait as a continuous measure within each jointly called VCF¹¹. Empiric kinship matrices were first generated for each VCF (“make-kin”) using default parameters. Next, association analyses (“single”) were performed adjusting for age, age², sex, cohort, self-reported ethnicity (for MESA), and an empirically derived kinship matrix to account for both familial and more distant relatedness within each VCF. For the TOPMed Phase I VCF, which included OOA, LDL-C and total cholesterol analyses were also adjusted for `APOB p.R3527Q` and triglycerides and HDL-C analyses were also adjusted for `APOC3 p.R19Ter`. To ensure robust results, we only performed single variant analysis for variants with a MAF $> 0.1\%$. Variants were meta-analyzed across all three VCFs using METAL (<https://genome.sph.umich.edu/wiki/METAL>)⁵¹. Summary statistics only for variants with MAF $> 0.1\%$ for the given VCF were included in the meta-analysis. Statistical significance α of 5×10^{-8} was used for these analyses.

For loci with at least one variant with $P < 5 \times 10^{-8}$ within the TOPMed Phase I VCF, iterative conditional association analysis was performed. Iterative conditioning was performed until $P > 1 \times 10^{-4}$ was attained.

Rare variant association analyses. We first identified rare (MAF $< 1\%$) mutations for each VCF within the coding sequences. After Variant Effect Predictor⁴⁹ annotation, we identified loss-of-function (e.g., nonsense, canonical splice-site, and frameshift) and disruptive missense (by MetaSVM¹⁰) in canonical transcripts as specified by Ensembl.

We further performed rare variant association tests within the non-coding space (Supplementary Figure 7). As before, we performed a “sliding window” approach aggregating 3 kb (overlapping by 1.5 kb) windows and considering rare variants occurring within enhancer or promoter elements at DNase I hypersensitivity sites.

For non-coding tests, we next attempted to link rare non-coding variants with genes for association testing using regulatory annotations for HepG2 and adipose nuclei from ENCODE and NIH Roadmap. Given prior observations showing enrichment of functional promoter variants at `LIPG` with HDL-C extremes⁵², we similarly aggregated variants near TSSs. Prior studies have shown that approximately 80% of cis-eQTLs fall within 100 kb of TSS⁵³. To increase the likelihood of mapping regulatory variants to the nearest gene, we were more restrictive and included variants overlapping promoter sequences ± 5 kb and enhancer sequences ± 20 kb of TSS at DNase I hypersensitivity sites.

We also linked chromatin state defined enhancers with genes using data from the Roadmap Epigenomics project⁵⁴ and the method presented previously⁵⁵ with a few small modifications⁵⁶. The method predicts links using chromatin state information, position of the enhancer relative to the TSS, and the correlation of multiple chromatin marks with gene expression across cell types. Here we used the correlation with gene expression of the signal of five chromatin marks: H3K27ac, H3K9ac, H3K4me1, H3K4me2, and DNaseI hypersensitivity. The gene expression data were the RPKM expression data for protein-coding exons across 56 reference epigenomes from the Roadmap Epigenomics project (available in the file `57epigenomes.RPKM.pc` from <http://compbio.mit.edu/roadmap>; Universal Human Reference was excluded). The chromatin mark signal was the $-\log_{10}(P)$ tracks averaged to a 200-bp resolution. As input to our code, we used the version of those tracks first averaged at 25-bp resolution using the “Convert” command of ChromImpute⁵⁷. In computing correlation between a specific chromatin mark signal and gene expression, we used the Pearson correlation and omitted from the calculation samples lacking both chromatin mark signal and gene expression data. We made predictions separately for each of the 127 reference epigenomes and locations assigned to chromatin states, `6_EnhG`, `7_Enh`, and `12_EnhBiv`, of the 15-state core 5-marks ChromHMM model^{54,58}. We restricted our predictions to chromatin state assignments on chr1–22 and chrX. We considered linking 200-bp bins within 1 Mb of a TSS of each gene as annotated in the file `Ensembl_v65.Gencode_v10.ENSEG.gene_info` available from <http://compbio.mit.edu/roadmap> (ref. 54). If a gene had multiple TSS, then we only used the outermost TSS.

The method for linking is based on determining for each combination of cell type, chromatin state, and position relative to the TSS the estimated probability the

set of correlations we observed would come from the actual data compared to randomized data. To this end, we created a training set of actual observed correlations (positive examples) and correlations computed after randomizing which gene expression values were assigned to which genes (negative examples) separately for each combination of cell type, chromatin state, and position relative to the TSS. Each entry in the training set has five features corresponding to correlations for each of the considered chromatin marks. There is a positive and a corresponding negative entry for each instance of the specified chromatin state in the specified cell type at the specified position relative to the TSS or within 5 kb of it (for smoothing purposes). We trained a logistic regression classifier to discriminate actual correlations with randomized correlations. We used the logistic regression library implemented in the Weka package version 3.7.3 with the regularization parameter set to 1⁵⁹. For considering linking a specific instance of a chromatin state assignment in a specific cell type and position relative to the TSS of a gene, we applied the corresponding classifier. Let p denote the probability the classifier gives of being in the positive class of the actual observed correlations. We retained those links for which $p/(1-p)$ was ≥ 2.5 . The method we used here is implemented in the code LinkingRM.java. For the analyses presented here, we used those links for the primary enhancer state, 7_Enh.

To connect non-coding variants with putative target genes, we predicted functional gene-enhancer pairs using a chromatin state-based model we previously developed¹⁵. This model assumes that the impact of an enhancer on gene expression is determined by the product of its intrinsic “Activity” (for which we use quantitative DNase-Seq and H3K27ac ChIP-Seq levels as a proxy) and the “Contact Frequency” at which the enhancer physically encounters its target promoter in the nucleus (for which we use Hi-C data as a proxy). We previously found such an Activity by Contact (ABC) model accurately identifies enhancers whose perturbation leads to changes in gene expression in the human MYC locus¹⁵, and we have since found that the same model can identify enhancers across other gene loci and cell types (Fulco, C., Lander, E., and Engreitz, J., in preparation). We extended our previously published model to predict enhancer-gene connections in the liver, using DNase-Seq and H3K27ac ChIP-Seq data from a hepatocarcinoma cell line (HepG2) previously generated by the ENCODE project⁶⁰. To define putative regulatory elements, we expanded DNase-Seq peak calls from ENCODE by 500 bp on either side and merged overlapping peaks¹⁵. For each element, we calculated Activity as a function of the normalized read count of H3K27ac and DNase-Seq. Because high-resolution Hi-C data is not available for HepG2 cells, we estimated the Contact probability between putative regulatory elements and genes using the average profile across deeply sequenced Hi-C libraries from seven different cell types⁶¹ as previously described¹⁵. For each putative enhancer-gene pair, we calculated an “ABC score” equal to the Activity \times Contact of the putative enhancer normalized by the sum of Activity \times Contact across all other putative elements within 5 Mb of the target gene. We tuned free parameters in this model (such as the relative weight of DNase-Seq and H3K27ac data and a pseudocount to add to Hi-C data) and chose a threshold cutoff using a set of experimentally measured enhancer-promoter connections in two cell types (Fulco, C., Lander, E., and Engreitz, J., in preparation). This analysis defined, for each expressed gene, a set of elements predicted to regulate that gene in HepG2 cells. These sets of elements were used for gene-level variant burden tests.

We tested the association of the aggregate MAF <1% variants within each of the aforementioned groupings with each lipid trait as continuous traits using the mixed-model SKAT implementation in EPACTS to account for bidirectional effects¹¹. We first created group files (“make-group”) using annotations from the aforementioned strategies, created VCF-specific kinship matrices (“make-kin”) using default parameters, and performed association analyses (“group --test mmskat -max-maf 0.01”) (<https://genome.sph.umich.edu/wiki/EPACTS>). Analyses were adjusted for age, age², sex, cohort, self-reported ethnicity (for MESA), and empiric kinship within each of the VCFs. P values for each grouping were meta-analyzed across the three cassettes using Fisher’s method. Statistical significance for each gene-based test was $0.05/20,000$ tests = 2.5×10^{-6} .

Lipid extremes analysis. We first defined LDL-C extremes as the top and bottom ancestry-specific 5th percentiles from the data (LDL-C >183 mg/dl or >198.6 mg/dl for EA and AA, respectively; LDL-C <72.9 mg/dl or <71 mg/dl for EA and AA, respectively).

We next cataloged mutations in Mendelian genes previously linked to extreme LDL-C (Supplementary Table 13). We included variants that were previously linked to Mendelian dyslipidemia in ClinVar (“pathogenic” or “likely pathogenic”) with no “benign”) or loss-of-function, and had an allele frequency <1% (autosomal dominant) or <10% (autosomal recessive). Genotypes were only considered based on expected inheritance pattern (autosomal dominant or autosomal recessive).

We evaluated three distinct approaches to generate weighted polygenic scores using prior genome-wide association analysis summary statistics⁷: (1) only lead variants at genome-wide significant loci, (2) varying P and LD r^2 thresholds (defined by 1000G CEU) using PLINK⁶², and (3) all variants but adjusting weights according to P and r^2 (by 1000G CEU) with LDpred varying rho¹⁶. To minimize errors from strand flips, A/T and C/G SNPs were excluded. The scores were calculated as additive sums of risk allele counts for included SNPs multiplied by weights (discovery effect estimates for (1) and (2), or adjusted by LDpred for (3)).

LDpred¹⁶ is a Bayesian approach, calculates a posterior mean effect size for each variant based on a prior (association with LDL-C in a previously published study) and subsequent shrinkage based on the extent to which this variant is correlated with similarly associated variants in a reference population. The underlying Gaussian distribution additionally considers the fraction of causal (e.g., non-zero effect sizes) markers. Because this fraction is unknown for any given disease, LDpred uses a range of plausible values to construct different polygenic scores.

Polygenic scores were generated within the HUNT cohort, the training set¹⁸. Lipid values were extracted from the electronic health record; absence of lipid-lowering therapy was prioritized. For each trait, the model with the best fit, as measured by R^2 , was chosen to apply to the testing set, TOPMed samples.

In a multivariable model, we associated likelihood of membership within the extreme tail of a trait with monogenic mutation carrier status, high (top 5th percentile) or low (bottom 5th percentile) polygenic score, age, age², and sex, separately in European American (EA from FHS and MESA-EA) and African American (AA from JHS and MESA-AA) samples. We also ran linear regression models with continuous LDL-C and the independent variables listed above.

Data availability. Individual whole-genome sequence data for TOPMed whole genomes (FHS, JHS, OOA, and MESA) are available through restricted access via the TOPMed dbGaP Exchange Area. The accession numbers are: FHS phs000974.v1.p1, JHS phs000964.v1.p1, OOA phs000956.v1.p1, and MESA phs001416.v1.p1. Individual-level harmonized lipids used for analysis are also available through restricted access via the TOPMed dbGaP Exchange Area. Summary-level genotype data are available through the BRAVO browser (<https://bravo.sph.umich.edu/>). The Finnish WGS and array genotype data can be accessed through the THL Biobank (<https://thl.fi/fi/web/thl-biobank>). The WGS data at Estonian Genome Center, University of Tartu, can be accessed via the Estonian Biobank (www.biobank.ee).

Received: 15 May 2018 Accepted: 22 June 2018

Published online: 23 August 2018

References

- Emerging Risk Factors C. et al. Major lipids, apolipoproteins, and risk of vascular disease. *JAMA* **302**, 1993–2000 (2009).
- Kathiresan, S. et al. A genome-wide association study for blood lipid phenotypes in the Framingham Heart Study. *BMC Med. Genet.* **8**(Suppl 1), S17 (2007).
- Fadista, J., Manning, A. K., Florez, J. C. & Groop, L. The (in)famous GWAS P-value threshold revisited and updated for low-frequency variants. *Eur. J. Hum. Genet.* **24**, 1202–1205 (2016).
- Kathiresan, S. et al. Common variants at 30 loci contribute to polygenic dyslipidemia. *Nat. Genet.* **41**, 56–65 (2009).
- Surakka, I. et al. The impact of low-frequency and rare variants on lipid levels. *Nat. Genet.* **47**, 589–597 (2015).
- Teslovich, T. M. et al. Biological, clinical and population relevance of 95 loci for blood lipids. *Nature* **466**, 707–713 (2010).
- Willer, C. J. et al. Discovery and refinement of loci associated with lipid levels. *Nat. Genet.* **45**, 1274–1283 (2013).
- Ripatti, P. et al. The contribution of GWAS loci in familial dyslipidemias. *PLoS Genet.* **12**, e1006078 (2016).
- Zuk, O. et al. Searching for missing heritability: designing rare variant association studies. *Proc. Natl Acad. Sci. USA* **111**, E455–E464 (2014).
- Dong, C. et al. Comparison and integration of deleteriousness prediction methods for nonsynonymous SNVs in whole exome sequencing studies. *Hum. Mol. Genet.* **24**, 2125–2137 (2015).
- Kang, H. M. et al. Variance component model to account for sample structure in genome-wide association studies. *Nat. Genet.* **42**, 348–354 (2010).
- Wu, M. C. et al. Rare-variant association testing for sequencing data with the sequence kernel association test. *Am. J. Hum. Genet.* **89**, 82–93 (2011).
- Morrison, A. C. et al. Practical approaches for whole-genome sequence analysis of heart- and blood-related traits. *Am. J. Hum. Genet.* **100**, 205–215 (2017).
- Morrison, A. C. et al. Whole-genome sequence-based analysis of high-density lipoprotein cholesterol. *Nat. Genet.* **45**, 899–901 (2013).
- Fulco, C. P. et al. Systematic mapping of functional enhancer-promoter connections with CRISPR interference. *Science* **354**, 769–773 (2016).
- Vilhjalmsson, B. J. et al. Modeling linkage disequilibrium increases accuracy of polygenic risk scores. *Am. J. Hum. Genet.* **97**, 576–592 (2015).
- Chatterjee, N. et al. Projecting the performance of risk prediction based on polygenic analyses of genome-wide association studies. *Nat. Genet.* **45**, 400–405 (2013). 405e401–403.

18. Holmen, O. L. et al. Systematic evaluation of coding variation identifies a candidate causal variant in *TMS6ZF* influencing total cholesterol and myocardial infarction risk. *Nat. Genet.* **46**, 345–351 (2014).
19. Kircher, M. et al. A general framework for estimating the relative pathogenicity of human genetic variants. *Nat. Genet.* **46**, 310–315 (2014).
20. Backenroth, D. et al. FUN-LDA: a latent dirichlet allocation model for predicting tissue-specific functional effects of noncoding variation: methods and applications. *Am. J. Human. Genet.* **102**, 920–942 (2018).
21. Lu, Q. et al. Systematic tissue-specific functional annotation of the human genome highlights immune-related DNA elements for late-onset Alzheimer's disease. *PLoS Genet.* **13**, e1006933 (2017).
22. Lu, Q., Powles, R. L., Wang, Q., He, B. J. & Zhao, H. Integrative tissue-specific functional annotations in the human genome provide novel insights on many complex traits and improve signal prioritization in genome wide association studies. *PLoS Genet.* **12**, e1005947 (2016).
23. Stitzel, N. O. et al. *ANGPTL3* deficiency and protection against coronary artery disease. *J. Am. Coll. Cardiol.* **69**, 2054–2063 (2017).
24. Thormaehlen, A. S. et al. Systematic cell-based phenotyping of missense alleles empowers rare variant association studies: a case for *LDLR* and myocardial infarction. *PLoS Genet.* **11**, e1004855 (2015).
25. Abul-Husn, N. S. et al. Genetic identification of familial hypercholesterolemia within a single U.S. health care system. *Science* **354**, pii: aaf7000 (2016).
26. Khera, A. V. et al. Diagnostic yield and clinical utility of sequencing familial hypercholesterolemia genes in patients with severe hypercholesterolemia. *J. Am. Coll. Cardiol.* **67**, 2578–2589 (2016).
27. Benn, M., Watts, G. F., Tybjaerg-Hansen, A. & Nordestgaard, B. G. Mutations causative of familial hypercholesterolemia: screening of 98 098 individuals from the Copenhagen General Population Study estimated a prevalence of 1 in 217. *Eur. Heart J.* **37**, 1384–1394 (2016).
28. Durst, R. et al. Molecular genetics of familial hypercholesterolemia in Israel-revisited. *Atherosclerosis* **257**, 55–63 (2017).
29. Mehta, R. et al. The panorama of familial hypercholesterolemia in Latin America: a systematic review. *J. Lipid Res.* **57**, 2115–2129 (2016).
30. Rabes, J. P., Beliard, S. & Carrie, A. Familial hypercholesterolemia: experience from France. *Curr. Opin. Lipidol.* **29**, 65–71 (2018).
31. Xiang, R. et al. The genetic spectrum of familial hypercholesterolemia in the central south region of China. *Atherosclerosis* **258**, 84–88 (2017).
32. Sharifi, M. et al. Greater preclinical atherosclerosis in treated monogenic familial hypercholesterolemia vs. polygenic hypercholesterolemia. *Atherosclerosis* **263**, 405–411 (2017).
33. Wang, J. et al. Polygenic versus monogenic causes of hypercholesterolemia ascertained clinically. *Arterioscler. Thromb. Vasc. Biol.* **36**, 2439–2445 (2016).
34. Zhan, X., Hu, Y., Li, B., Abecasis, G. R. & Liu, D. J. RVTESTS: an efficient and comprehensive tool for rare variant association analysis using sequence data. *Bioinformatics* **32**, 1423–1426 (2016).
35. Feng, S., Liu, D., Zhan, X., Wing, M. K. & Abecasis, G. R. RAREMETAL: fast and powerful meta-analysis for rare variants. *Bioinformatics* **30**, 2828–2829 (2014).
36. Martin, A. R. et al. Human demographic history impacts genetic risk prediction across diverse populations. *Am. J. Hum. Genet.* **100**, 635–649 (2017).
37. Botigue, L. R. et al. Gene flow from North Africa contributes to differential human genetic diversity in southern Europe. *Proc. Natl Acad. Sci. USA* **110**, 11791–11796 (2013).
38. Qin, P. et al. Quantitating and dating recent gene flow between European and East Asian populations. *Sci. Rep.* **5**, 9500 (2015).
39. Marquez-Luna, C., Loh, P. R., South Asian Type 2 Diabetes (SAT2D) Consortium, SIGMA Type 2 Diabetes Consortium & Price, A. L. Multiethnic polygenic risk scores improve risk prediction in diverse populations. *Genet. Epidemiol.* **41**, 811–823 (2017).
40. Jun, G., Wing, M. K., Abecasis, G. R. & Kang, H. M. An efficient and scalable analysis framework for variant extraction and refinement from population-scale DNA sequence data. *Genome Res.* **25**, 918–925 (2015).
41. Jun, G. et al. Detecting and estimating contamination of human DNA samples in sequencing and array-based genotype data. *Am. J. Hum. Genet.* **91**, 839–848 (2012).
42. Tan, A., Abecasis, G. R. & Kang, H. M. Unified representation of genetic variants. *Bioinformatics* **31**, 2202–2204 (2015).
43. Li, B. & Leal, S. M. Methods for detecting associations with rare variants for common diseases: application to analysis of sequence data. *Am. J. Hum. Genet.* **83**, 311–321 (2008).
44. Li, H. & Durbin, R. Fast and accurate short read alignment with Burrows-Wheeler transform. *Bioinformatics* **25**, 1754–1760 (2009).
45. Van der Auwera GA. et al. From FastQ data to high confidence variant calls: the Genome Analysis Toolkit best practices pipeline. *Curr. Protoc. Bioinformatics* **11**, 11 10 11–11 10 33 (2013).
46. Cingolani, P. et al. A program for annotating and predicting the effects of single nucleotide polymorphisms, SnpEff: SNPs in the genome of *Drosophila melanogaster* strain w1118; iso-2; iso-3. *Fly* **6**, 80–92 (2012).
47. Ganna, A. et al. Ultra-rare disruptive and damaging mutations influence educational attainment in the general population. *Nat. Neurosci.* **19**, 1563–1565 (2016).
48. Li, H. Toward better understanding of artifacts in variant calling from high-coverage samples. *Bioinformatics* **30**, 2843–2851 (2014).
49. McLaren, W. et al. Deriving the consequences of genomic variants with the Ensembl API and SNP Effect Predictor. *Bioinformatics* **26**, 2069–2070 (2010).
50. Peloso, G. M. et al. Association of low-frequency and rare coding-sequence variants with blood lipids and coronary heart disease in 56,000 whites and blacks. *Am. J. Hum. Genet.* **94**, 223–232 (2014).
51. Willer, C. J., Li, Y. & Abecasis, G. R. METAL: fast and efficient meta-analysis of genomewide association scans. *Bioinformatics* **26**, 2190–2191 (2010).
52. Khetarpal, S. A. et al. Mining the LIPG allelic spectrum reveals the contribution of rare and common regulatory variants to HDL cholesterol. *PLoS Genet.* **7**, e1002393 (2011).
53. Consortium, G. T. Human genomics. The Genotype-Tissue Expression (GTEx) pilot analysis: multitissue gene regulation in humans. *Science* **348**, 648–660 (2015).
54. Zhou, X. et al. Epigenomic annotation of genetic variants using the Roadmap Epigenome Browser. *Nat. Biotechnol.* **33**, 345–346 (2015).
55. Ernst, J. et al. Mapping and analysis of chromatin state dynamics in nine human cell types. *Nature* **473**, 43–49 (2011).
56. Liu, Y., Sarkar, A., Kheradpour, P., Ernst, J. & Kellis, M. Evidence of reduced recombination rate in human regulatory domains. *Genome Biol.* **18**, 193 (2017).
57. Ernst, J. & Kellis, M. Large-scale imputation of epigenomic datasets for systematic annotation of diverse human tissues. *Nat. Biotechnol.* **33**, 364–376 (2015).
58. Ernst, J. & Kellis, M. ChromHMM: automating chromatin-state discovery and characterization. *Nat. Methods* **9**, 215–216 (2012).
59. Frank, E., Hall, M., Trigg, L., Holmes, G. & Witten, I. H. Data mining in bioinformatics using Weka. *Bioinformatics* **20**, 2479–2481 (2004).
60. Consortium, E. P. An integrated encyclopedia of DNA elements in the human genome. *Nature* **489**, 57–74 (2012).
61. Rao, S. S. et al. A 3D map of the human genome at kilobase resolution reveals principles of chromatin looping. *Cell* **159**, 1665–1680 (2014).
62. Purcell, S. et al. PLINK: a tool set for whole-genome association and population-based linkage analyses. *Am. J. Hum. Genet.* **81**, 559–575 (2007).

Acknowledgements

WGS for the Trans-Omics in Precision Medicine (TOPMed) program was supported by the National Heart, Lung and Blood Institute (NHLBI). WGS for “NHLBI TOPMed: Whole Genome Sequencing and Related Phenotypes in the Framingham Heart Study” (phs000974.v1.p1) was performed at the Broad Institute of MIT and Harvard (HHSN268201500014C). WGS for “NHLBI TOPMed: The Jackson Heart Study” (phs000964.v1.p1) was performed at the University of Washington Northwest Genomics Center (HHSN268201100037C). WGS for “NHLBI TOPMed: Genetics of Cardiometabolic Health in the Amish” (phs000956.v1.p1) was performed at the Broad Institute of MIT and Harvard (3R01HL121007-01S1). WGS for “NHLBI TOPMed: Multi-Ethnic Study of Atherosclerosis (MESA)” (phs001416.v1.p1) was performed at the Broad Institute of MIT and Harvard (3U54HG003067-13S1). Centralized read mapping and genotype calling, along with variant quality metrics and filtering, were provided by the TOPMed Informatics Research Center (3R01HL-117626-02S1). Phenotype harmonization, data management, sample-identity QC, and general study coordination were provided by the TOPMed Data Coordinating Center (3R01HL-120393-02S1). We gratefully acknowledge the studies and participants who provided biological samples and data for TOPMed. Further study-specific acknowledgements can be found in Supplementary Note 2. This analysis was supported by the American Heart Association 17SDG33680041 (P.N.), the National Heart, Lung, and Blood Institute of the US National Institutes of Health grants K01 HL125751 (G.M.P.), R01 HL127564 (C.W. and S.K.), and TOPMed analysis support grant (G.M.P. and P.N.), the Ofer and Shelly Nemirovsky Research Scholar award from Massachusetts General Hospital (S.K.), and the Donovan Family Foundation (S.K.). The sponsors had no role in the design and conduct of the study; collection, management, analysis, and interpretation of the data; preparation, review, or approval of the manuscript; and decision to submit the manuscript for publication.

Author contributions

P.N., G.M.P., S.M.Z., G.A., J.G.W., L.A.C., C.J.W., and S.K. designed the study. P.N., G.M.P., S.M.Z., M.M., A.G., M.C., A.V.K., W.Z., J.B., J.R.O., J.M.E., J.E., A.M., W.C.J., T.P., C.S., V.S., R.S.V., M.K., E.S.L., S.E.R., M.A., J.A.P., I.L.S., T.E., S.R., A.C., B.N., G.A., B.M., S.S.R., J.G.W., L.A.C., J.I.R., C.J.W., and S.K. acquired, analyzed or interpreted data. P.N., G.M.P., S.M.Z., M.M., A.G., S.R., B.M., S.S.R., J.G.W., L.A.C., J.I.R., C.J.W., and S.K. wrote

the manuscript. P.N., G.M.P., S.K., and NHLBI TOPMed Lipids Working Group provided administrative, technical or material support.



Open Access This article is licensed under a Creative Commons Attribution 4.0 International License, which permits use, sharing, adaptation, distribution and reproduction in any medium or format, as long as you give appropriate credit to the original author(s) and the source, provide a link to the Creative Commons license, and indicate if changes were made. The images or other third party material in this article are included in the article's Creative Commons license, unless indicated otherwise in a credit line to the material. If material is not included in the article's Creative Commons license and your intended use is not permitted by statutory regulation or exceeds the permitted use, you will need to obtain permission directly from the copyright holder. To view a copy of this license, visit <http://creativecommons.org/licenses/by/4.0/>.

Additional information

Supplementary Information accompanies this paper at <https://doi.org/10.1038/s41467-018-05747-8>.

Competing interests: The authors declare no competing interests.

Reprints and permission information is available online at <http://npg.nature.com/reprintsandpermissions/>

Publisher's note: Springer Nature remains neutral with regard to jurisdictional claims in published maps and institutional affiliations.

© The Author(s) 2018

NHLBI TOPMed Lipids Working Group

Namiko Abe²⁵, Christine Albert²⁶, Nicholette (Nichole) Palmer Allred²⁷, Laura Almasy^{28,29}, Alvaro Alonso³⁰, Seth Ament³¹, Peter Anderson³², Pramod Anugu³³, Deborah Applebaum-Bowden³⁴, Dan Arking³⁵, Donna K Arnett³⁶, Allison Ashley-Koch³⁷, Stella Aslibekyan³⁸, Tim Assimes³⁹, Paul Auer⁴⁰, Dimitrios Avramopoulos³⁵, John Barnard⁴¹, Kathleen Barnes⁴², R. Graham Barr⁴³, Emily Barron-Casella³⁵, Terri Beaty³⁵, Diane Becker³⁵, Lewis Becker³⁵, Rebecca Beer³⁴, Ferdouse Begum³⁵, Amber Beitelshees³¹, Emelia Benjamin^{44,26}, Marcos Bezerra⁴⁵, Larry Bielak⁴⁶, Joshua Bis³², Thomas Blackwell⁴⁶, John Blangero⁴⁷, Eric Boerwinkle⁴⁸, Ingrid Borecki³², Russell Bowler⁴⁹, Jennifer Brody³², Ulrich Broeckel⁵⁰, Jai Broome³², Karen Bunting²⁵, Esteban Burchard⁵¹, Jonathan Cardwell⁴², Cara Carty⁵², Richard Casaburi⁵³, James Casella³⁵, Christy Chang³¹, Daniel Chasman⁵⁴, Sameer Chavan⁴², Bo-Juen Chen²⁵, Wei-Min Chen⁵⁵, Yii-Der Ida Chen⁵⁶, Michael Cho⁵⁴, Seung Hoan Choi⁵⁷, Lee-Ming Chuang⁵⁸, Mina Chung⁴¹, Elaine Cornell⁵⁹, Carolyn Crandall⁵³, James Crapo⁴⁹, Joanne Curran⁴⁷, Jeffrey Curtis⁴⁶, Brian Custer⁶⁰, Coleen Damcott³¹, Dawood Darbar⁶¹, Sayantan Das⁴⁶, Sean David³⁹, Colleen Davis³², Michelle Daya⁴², Mariza de Andrade⁶², Michael DeBaun⁶³, Ranjan Deka⁶⁴, Dawn DeMeo⁵⁴, Scott Devine³¹, Ron Do⁶⁵, Qing Duan⁶⁶, Ravi Duggirala⁶⁷, Peter Durda⁵⁹, Susan Dutcher⁶⁸, Charles Eaton⁶⁹, Lynette Ekunwe³³, Patrick Ellinor²⁶, Leslie Emery³², Charles Farber⁵⁵, Leanna Farnam⁵⁴, Tasha Fingerlin⁴⁹, Matthew Flickinger⁴⁶, Myriam Fornage⁴⁸, Nora Franceschini⁶⁶, Mao Fu³¹, Malia Fullerton³², Lucinda Fulton⁶⁸, Stacey Gabriel⁵⁷, Weiniu Gan³⁴, Yan Gao³³, Margery Gass⁷⁰, Bruce Gelb⁶⁵, Xiaoqi (Priscilla) Geng⁴⁶, Soren Germer²⁵, Chris Gignoux³⁹, Mark Gladwin⁷¹, David Glahn⁷², Stephanie Gogarten³², Da-Wei Gong³¹, Harald Goring⁷³, C. Charles Gu⁶⁸, Yue Guan³¹, Xiuqing Guo⁵⁶, Jeff Haessler^{70,52}, Michael Hall³³, Daniel Harris³¹, Nicola Hawley⁷², Jiang He⁷⁴, Ben Heavner³², Susan Heckbert³², Ryan Hernandez⁵¹, David Herrington²⁷, Craig Hersh⁵⁴, Bertha Hidalgo³⁸, James Hixson⁴⁸, John Hokanson⁴², Elliott Hong³¹, Karin Hoth⁷⁵, Chao (Agnes) Hsiung⁷⁶, Haley Huston⁷⁷, Chii Min Hwu⁷⁸, Marguerite Ryan Irvin³⁸, Rebecca Jackson⁷⁹, Deepti Jain³², Cashell Jaquish³⁴, Min A Jhun⁴⁶, Jill Johnsen^{80,32}, Andrew Johnson⁸¹, Rich Johnston³⁰, Kimberly Jones³⁵, Hyun Min Kang⁴⁶, Robert Kaplan⁸², Sharon Kardia⁴⁶, Laura Kaufman⁵⁴, Shannon Kelly⁶⁰, Eimear Kenny⁶⁵, Michael Kessler³¹, Alyna Khan³², Greg Kinney⁴², Barbara Konkle⁸³, Charles Kooperberg⁷⁰, Holly Kramer⁸⁴, Stephanie Krauter³², Christoph Lange⁸⁵, Ethan Lange⁴², Leslie Lange⁴², Cathy Laurie³², Cecelia Laurie³², Meryl LeBoff⁵⁴, Seunggeun Shawn Lee⁴⁶, Wen-Jane Lee⁷⁸, Jonathon LeFaive⁴⁶, David Levine³², Dan Levy⁸¹, Joshua Lewis³¹, Yun Li⁶⁶, Honghuang Lin⁴⁴, Keng Han Lin⁴⁶, Simin Liu^{69,52}, Yongmei Liu²⁷, Ruth Loos⁶⁵, Steven Lubitz²⁶, Kathryn Lunetta⁴⁴, James Luo⁸¹, Michael Mahaney⁴⁷, Barry Make³⁵, JoAnn Manson⁵⁴, Lauren Margolin⁵⁷, Lisa Martin⁸⁶, Susan Mathai⁴²,

Rasika Mathias³⁵, Patrick McArdle³¹, Merry-Lynn McDonald³⁸, Sean McFarland⁸⁷, Stephen McGarvey⁶⁹, Hao Mei³³, Deborah A Meyers⁸⁸, Julie Mikulla³⁴, Nancy Min³³, Mollie Minear³⁴, Ryan L Minster⁷¹, Solomon Musani³³, Stanford Mwasongwe³³, Josyf C Mychaleckyj⁵⁵, Girish Nadkarni⁶⁵, Rakhi Naik³⁵, Sergei Nekhai⁸⁹, Deborah Nickerson³², Kari North⁶⁶, Tim O'Connor³¹, Heather Ochs-Balcom⁹⁰, James Pankow⁹¹, George Papanicolaou³⁴, Margaret Parker⁵⁴, Afshin Parsa³¹, Sara Penchev⁴⁹, Juan Manuel Peralta⁶⁷, Marco Perez³⁹, Ulrike Peters^{70,32}, Patricia Peyser⁴⁶, Larry Phillips³⁰, Sam Phillips³², Toni Pollin³¹, Wendy Post³⁵, Julia Powers Becker⁴², Meher Preethi Boorgula⁴², Michael Preuss⁶⁵, Dmitry Prokopenko⁸⁷, Bruce Psaty³², Pankaj Qasba³⁴, Dandi Qiao⁵⁴, Zhaohui Qin³⁰, Nicholas Rafaels⁴², Laura Raffield⁶⁶, D.C. Rao⁶⁸, Laura Rasmussen-Torvik⁹², Aakrosh Ratan⁵⁵, Susan Redline⁵⁴, Robert Reed³¹, Elizabeth Regan⁴⁹, Alex Reiner^{70,32}, Ken Rice³², Dan Roden⁶³, Carolina Roselli⁵⁷, Ingo Ruczinski³⁵, Pamela Russell⁴², Sarah Ruuska⁹³, Kathleen Ryan³¹, Phuwanat Sakornsakolpat⁵⁴, Shabnam Salimi³¹, Steven Salzberg³⁵, Kevin Sandow⁵⁶, Vijay Sankaran⁸⁷, Ellen Schmidt⁴⁶, Karen Schwander⁶⁸, David Schwartz⁴², Frank Sciorba⁷¹, Christine Seidman⁹⁴, Vivien Sheehan⁹⁵, Amol Shetty³¹, Aniket Shetty⁴², Wayne Hui-Heng Sheu⁷⁸, M. Benjamin Shoemaker⁶³, Brian Silver⁹⁶, Edwin Silverman⁵⁴, Jennifer Smith⁴⁶, Josh Smith³², Nicholas Smith³², Tanja Smith²⁵, Sylvia Smoller⁸², Beverly Snively²⁷, Tamar Sofer⁵⁴, Nona Sotodehnia³², Adrienne Stilp³², Elizabeth Streeten³¹, Yun Ju Sung⁶⁸, Jody Sylvia⁵⁴, Adam Szpiro³², Carole Sztalryd³¹, Daniel Taliun⁴⁶, Hua Tang³⁹, Margaret Taub³⁵, Kent Taylor⁵⁶, Simeon Taylor³¹, Marilyn Telen³⁷, Timothy A. Thornton³², Lesley Tinker⁵², David Tirschwell³², Hemant Tiwari³⁸, Russell Tracy⁵⁹, Michael Tsai⁹¹, Dhananjay Vaidya³⁵, Peter VandeHaar⁴⁶, Scott Vrieze^{97,91}, Tarik Walker⁴², Robert Wallace⁷⁵, Avram Walts⁴², Emily Wan⁵⁴, Fei Fei Wang³², Karol Watson⁵³, Daniel E. Weeks⁷¹, Bruce Weir³², Scott Weiss⁵⁴, Lu-Chen Weng²⁶, Cristen Willer⁴⁶, Kayleen Williams³², L. Keoki Williams⁹⁸, Carla Wilson⁵⁴, Quenna Wong³², Huichun Xu³¹, Lisa Yanek³⁵, Ivana Yang⁴², Rongze Yang³¹, Norann Zaghoul³¹, Yingze Zhang⁷¹, Snow Xueyan Zhao⁴⁹, Xiuwen Zheng³², Degui Zhi⁴⁸, Xiang Zhou⁴⁶, Michael Zody²⁵ & Sebastian Zoellner⁴⁶

²⁵New York Genome Center, New York, NY 10013, USA. ²⁶Massachusetts General Hospital, Boston, MA 02114, USA. ²⁷Wake Forest Baptist Health, Winston-Salem, NC 27157, USA. ²⁸Children's Hospital of Philadelphia, Philadelphia, PA 19104, USA. ²⁹University of Pennsylvania, Philadelphia, PA 19104, USA. ³⁰Emory University, Atlanta, GA 30322, USA. ³¹University of Maryland School of Medicine, Baltimore, MD 21201, USA. ³²University of Washington, Seattle, WA 98195, USA. ³³University of Mississippi, Jackson, MS 38677, USA. ³⁴National Institutes of Health, Bethesda, MD 20892, USA. ³⁵Johns Hopkins University, Baltimore, MD 21218, USA. ³⁶University of Kentucky, Lexington, KY 40506, USA. ³⁷Duke University, Durham, NC 27708, USA. ³⁸University of Alabama, Birmingham, AL 35487, USA. ³⁹Stanford University, Stanford, CA 94305, USA. ⁴⁰University of Wisconsin Milwaukee, Milwaukee, WI 53211, USA. ⁴¹Cleveland Clinic, Cleveland, OH 44195, USA. ⁴²University of Colorado at Denver, Denver, CO 80204, USA. ⁴³Columbia University, New York, NY 10027, USA. ⁴⁴Boston University, Boston, MA 02215, USA. ⁴⁵Fundação de Hematologia e Hemoterapia de Pernambuco - Hemope, Recife 52011-000, Brazil. ⁴⁶University of Michigan, Ann Arbor, MI 48109, USA. ⁴⁷University of Texas Rio Grande Valley School of Medicine, Brownsville, TX 78520, USA. ⁴⁸University of Texas Health, Houston, TX 77225, USA. ⁴⁹National Jewish Health, Denver, CO 80206, USA. ⁵⁰Medical College of Wisconsin, Milwaukee, WI 53226, USA. ⁵¹University of California, San Francisco, San Francisco, CA 94143, USA. ⁵²Women's Health Initiative, Seattle, WA 98109, USA. ⁵³University of California, Los Angeles, Los Angeles, CA 90095, USA. ⁵⁴Brigham & Women's Hospital, Boston, MA 02115, USA. ⁵⁵University of Virginia, Charlottesville, VA 22903, USA. ⁵⁶Los Angeles Biomedical Research Institute, Los Angeles, CA 90502, USA. ⁵⁷The Broad Institute, Cambridge, MA 02142, USA. ⁵⁸National Taiwan University, 10617 Taipei, Taiwan. ⁵⁹University of Vermont, Burlington, VT 05405, USA. ⁶⁰Blood Systems Research Institute UCSF, San Francisco, CA 94118, USA. ⁶¹University of Illinois at Chicago, Chicago, IL 60607, USA. ⁶²Mayo Clinic, Rochester, MN 55905, USA. ⁶³Vanderbilt University, Nashville, TN 37235, USA. ⁶⁴University of Cincinnati, Cincinnati, OH 45220, USA. ⁶⁵Icahn School of Medicine at Mount Sinai, New York 10029 NY, USA. ⁶⁶University of North Carolina, Chapel Hill, NC 27599, USA. ⁶⁷University of Texas Rio Grande Valley School of Medicine, Edinburg, TX 78539, USA. ⁶⁸Washington University in St Louis, St Louis, MO 63130, USA. ⁶⁹Brown University, Providence, RI 02912, USA. ⁷⁰Fred Hutchinson Cancer Research Center, Seattle, WA 98109, USA. ⁷¹University of Pittsburgh, Pittsburgh, PA 15260, USA. ⁷²Yale University, New Haven, CT 06520, USA. ⁷³University of Texas Rio Grande Valley School of Medicine, San Antonio, TX 78229, USA. ⁷⁴Tulane University, New Orleans, LA 70118, USA. ⁷⁵University of Iowa, Iowa City, IA 52242, USA. ⁷⁶National Health Research Institute Taiwan, 350 Zhunan Township, Taiwan. ⁷⁷Blood Works Northwest, Seattle, WA 98105, USA. ⁷⁸Taichung Veterans General Hospital Taiwan, 407 Taichung City, Taiwan. ⁷⁹Ohio State University Wexner Medical Center, Columbus, OH 43210, USA. ⁸⁰Blood Works Northwest, Seattle, WA 98106, USA. ⁸¹NIH National Heart, Lung, and Blood Institute, Bethesda, MD 20892, USA. ⁸²Albert Einstein College of Medicine, New York, NY 10461, USA. ⁸³Blood Works Northwest, Seattle, WA 98104, USA. ⁸⁴Loyola University, Maywood, IL 60153, USA. ⁸⁵Harvard School of Public Health, Boston, MA 02115, USA. ⁸⁶George Washington University, Washington, DC 20052, USA. ⁸⁷Harvard University, Cambridge, MA 02138, USA. ⁸⁸University of Arizona, Tucson, AZ 85721, USA. ⁸⁹Howard University, Washington, DC 20059, USA. ⁹⁰University at Buffalo, Buffalo, NY 14260, USA. ⁹¹University of Minnesota, Minneapolis, MN 55455, USA. ⁹²Northwestern University, Chicago, IL 60208, USA. ⁹³Blood Works Northwest, Seattle, WA 98107, USA. ⁹⁴Harvard Medical School, Boston, MA 02115, USA. ⁹⁵Baylor College of Medicine, Houston, TX 77030, USA. ⁹⁶UMass Memorial Medical Center, Worcester, MA 01655, USA. ⁹⁷University of Colorado at Boulder, Boulder, CO 80309, USA. ⁹⁸Henry Ford Health System, Detroit, MI 48202, USA